Regular Article

Optimized film thicknesses for maximum refractive index sensitivity and figure of merit of a bimetallic film surface plasmon resonance sensor

Jakub Chylek[a] , **Dalibor Ciprian, Petr Hlubina**

Department of Physics, Technical University of Ostrava, 17. listopadu 2172/15, 708 00 Ostrava-Poruba, Czech Republic

Abstract In this paper, a simple surface plasmon resonance (SPR) optical sensor with a bimetallic gold-silver film is proposed and its parameters are optimized based on reflectance spectra analysis. In comparison with most SPR sensors, which use single gold films, the evanescent field of this bimetallic configuration at the analyte–metal interface enables the sensing with substantially enhanced refractive index (RI) sensitivity and figure of merit (FOM). The proposed structure comprising a BK7 glass substrate, an adhesion layer of chromium, a gold-silver plasmonic layer, and a protective layer of silicon dioxide is employed in the Kretschmann configuration for liquid analyte sensing. In order to achieve the best sensing properties, the gold-silver layer thickness ratio is varied, and a thorough analysis of reflectance spectra is performed based on RI sensitivity and FOM. For this purpose, a liquid analyte of aqueous solutions of NaCl is employed for angles of incidence 63° and 64°, respectively. Moreover, based on the analysis, an optimized gold-silver layer thickness ratio is selected, and a sensitivity of 41,592 nm per RI unit (RIU) and FOM of 424 RIU^{-1} are reached. The designed bimetallic SPR structure proves to be advantageous compared to single-gold-film structures employed for sensing applications.

1 Introduction

Across numerous branches of science, the surface plasmon resonance (SPR) phenomenon has found its purpose primarily for sensing due to its high sensitivity to the refractive index (RI) of the surrounding medium [1–4]. The SPR sensing capitalizes on intensity [5] or phase [6] detection, which is either based on spectral [7–10] or angular interrogation techniques [8, 11]. The sensing properties of an SPR structure belong to the key factors determining the sensor performance. The structural parameters and optical properties, which are the defining elements of the utilized structure, significantly affect the sensing properties. Thus, intense focus is put on the appropriate selection of the plasmonic materials and architectural features of the SPR structures to increase the sensor capability.

A promising approach to enhance the sensor performance is to utilize a bimetallic configuration [12]. In this regard, various studies tackling this approach employing a detection technique based on the angular interrogation have been published. Despite the bimetallic configuration of Au–Ag being the most common due to its properties, a combination of metals such as Al–Au has been utilized [13]. Furthermore, bimetallic configurations of Cu–Ni or Al–Ni were employed together with two-dimensional (2D) materials to enhance the sensitivity of the sensor [14, 15]. 2D material structures are well-represented components of the SPR-based biosensors. Broad theoretical analysis of the Au–Ag or Ag–Au bimetallic configurations employed in the Kretschmann configuration [16–19] was performed, which included graphene, WS_2 or MoS_2. Moreover, an alternative to those materials, black phosphorus, has been successfully employed in bimetallic plasmonic biosensor for urine glucose detection [20]. Similarly, very high angular sensitivity of 360° per RI unit (RIU), 299°/RIU, and 378°/RIU was reached for the bimetallic configuration of Ag, Au and Cu in combination with barium titanate while also employing the black phosphorus [21]. Additionally, a thorough study of bimetallic and nanoparticle alloy combinations on the performance of SPR-based fiber optic sensors employing a detection technique based on the spectral interrogation has been reported [22–24].

Ultimately, the plasmonic layer and its thickness shape the resonance dip in the reflectance spectrum and dictate its properties. Therefore, it is pivotal to optimize the bimetallic layer thickness to achieve the best sensing performance when the angular interrogation is employed [25–27]. Similar problems arise when the spectral interrogation is employed, and consequently, the optimization method presented in this paper is found on the dip parameters interrogation.

In this paper, we propose a simple design of a surface plasmon resonance-based structure with a gold-silver plasmonic layer and a protective layer of silicon dioxide. It is advantageous to consider bimetallic plasmonic film as opposed to a single metal plasmonic layer, as in particular cases, the evanescent field of this bimetallic configuration can lead to sensing with substantially enhanced RI

---

[a] e-mail: jakub.chylek@vsb.cz (corresponding author)

sensitivity and figure of merit (FOM). The proposed structure is employed for liquid analyte sensing in the Kretschmann configuration, and aqueous solutions of NaCl with varying mass concentrations of NaCl in water in a range of 0–10 wt% are considered. A thorough reflectance spectra analysis is performed based on RI sensitivity and FOM in a spectral region of 1000–1900 nm for two angles of incidence $\theta = 63°$ and $\theta = 64°$, respectively. For each angle of incidence the reflectance response of the SPR structure is computed for combination of gold and silver layer thicknesses and aqueous NaCl solutions. The spectra are evaluated by an automated script, which provides a surface plot as a final output of RI sensitivity, depth of the dip and FOM as a function of the thicknesses of both gold and silver layers.

Furthermore, based on the analysis, a structure comprising the gold layer with a thickness of 40 nm and the silver layer with a thickness of 8 nm was selected. Theoretical spectral reflectance for p polarized waves for these structural parameters is computed and is further analyzed. Moreover, the sensing properties of an optimized structure are determined, and a sensitivity of 41,592 nm per RIU and FOM of 424 RIU^{-1} are reached. Additionally, to provide a more detailed description of the SPR effect at this bimetallic configuration at the analyte–metal interface, normalized optical field intensities are computed together with the field distributions in the structure. The results shown in the paper exhibit a substantial improvement in the same spectral region over the structure with a single gold film previously studied in [28].

2 Structure characterization

The proposed structure consists of a BK7 glass substrate, an adhesion chromium layer, a bimetallic gold-silver layer, and a protective layer of silicon dioxide (SiO$_2$). The structure is drawn schematically in Fig. 1.

2.1 Transfer matrix method

The optical response of a multilayer structure in the Kretschmann configuration can be expressed using the transfer matrix method (TMM). The propagation of electromagnetic waves through a system of thin layers can be described with the use of transmission and propagation matrices for individual layers. The transmission matrix $\mathbf{D}_{ij}$ at the ij-th interface (for $i = j - 1$) can be defined as [29]:

$$\mathbf{D}_{ij} = \frac{1}{t_{ij}} \begin{bmatrix} 1 & r_{ij} \\ r_{ij} & 1 \end{bmatrix}. \tag{1}$$

Furthermore, the propagation matrix $\mathbf{P}_j$ through the j-th layer can be defined as:

$$\mathbf{P}_j = \begin{bmatrix} e^{ik_j t_j} & 0 \\ 0 & e^{-ik_j t_j} \end{bmatrix}, \tag{2}$$

where t_j denotes a layer thickness and k_j denotes a wave-vector component in perpendicular alignment to the ij-th interface. In the case of prism-based coupling, the incident light can be expressed as:

$$k_j(\lambda) = \frac{2\pi}{\lambda} \left[n_j^2(\lambda) - n_p^2(\lambda) \sin^2 \theta \right]^{1/2}, \tag{3}$$

where $n_p(\lambda)$ is the refractive index of the prism and θ is the angle of incidence. By linking together transmission and propagation matrices across the entire structure, the total transfer matrix $\mathbf{M}$ can be obtained:

$$\mathbf{M} = \left[\prod_{j=1}^{N} \mathbf{D}_{ij} \mathbf{P}_j \right] \mathbf{D}_{N,N+1} = \begin{bmatrix} M_{11} & M_{12} \\ M_{21} & M_{22} \end{bmatrix}. \tag{4}$$
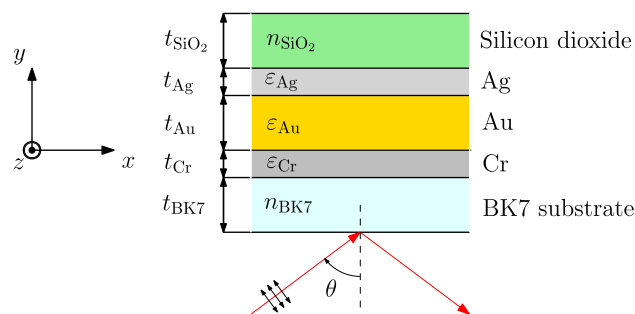
Fig. 1 Schematic drawing of a bimetallic plasmonic structure

The reflection coefficient r can be expressed using the total transfer matrix elements

$$r = \frac{M_{21}}{M_{11}}, \tag{5}$$

and the spectral reflectance $R_p(\lambda)$ of p polarization can be calculated as

$$R_p(\lambda) = \left| r_p(\lambda) \right|^2. \tag{6}$$

2.2 Material characterization

This section includes all the necessary dispersion formulas and parameters used to model the optical response of the multilayer structure.

2.2.1 Silicon dioxide, BK7 glass

The refractive index of SiO_2 and the BK7 glass (both a prism and substrate) as a function of wavelength can be described by a three-term Sellmeier formula [30, 31]:

$$n^2(\lambda) = 1 + \sum_{i=1}^{3} \frac{A_i \lambda^2}{\lambda^2 - B_i}, \tag{7}$$

where λ is the wavelength in μm. The values of Sellmeier coefficients for SiO_2 at the room temperature are as follows: $A_1 = 0.6961663$, $A_2 = 0.4079426$, $A_3 = 0.8974794$, $B_1 = 0.0684043 \, \mu m^2$, $B_2 = 0.1162414 \, \mu m^2$, $B_3 = 9.896161 \, \mu m^2$. Similarly, for the BK7 glass with the values of Sellmeier coefficients at the room temperature [31]: $A_1 = 1.03961212$, $A_2 = 2.31792344 \times 10^{-1}$, $A_3 = 1.01046945$, $B_1 = 6.00069867 \times 10^{-3} \mu m^2$, $B_2 = 2.00179144 \times 10^{-2} \mu m^2$ and $B_3 = 1.03560653 \times 10^2 \, \mu m^2$.

2.2.2 Gold, silver

The dispersion of the gold and silver layer can be described by the complex dielectric function given by the Drude–Lorentz model [32]:

$$\varepsilon_{Au/Ag}(\lambda) = \varepsilon_\infty - \frac{1}{\lambda_p^2(1/\lambda^2 + i/\gamma_p \lambda)} - \sum_{j=1}^{n} \frac{A_j}{\lambda_j^2(1/\lambda^2 - 1/\lambda_j^2) + i\lambda_j^2/\gamma_j \lambda}, \tag{8}$$

with the parameters listed in Table 1 for gold, and in Table 2 for silver.

Table 1 Parameters of the Drude–Lorentz dispersion formula for gold [33]

Parameter	Drude term			Oscillator		
	ϵ_∞	λ_p (nm)	γ_p (nm)	A_j	λ_j (nm)	γ_j (nm)
Value 1	1	133.85	27851	3.612	309.11	2591.3
Value 2				1.423	424.06	1515.2

Table 2 Parameters of the Drude–Lorentz dispersion formula for silver [34]

Parameter	Drude term			Oscillator		
	ϵ_∞	λ_p (nm)	γ_p (nm)	A_j	λ_j (nm)	γ_j (nm)
Value 1	1	149.67	25830	7.925	1519.41	319.05
Value 2				0.501	276.69	2743.01
Value 3				0.013	151.48	19074.49
Value 4				0.827	136.5	1353.54
Value 5				1.113	61.11	512.54

Parameter	Drude term			CP term			
	ϵ_∞	λ_p (nm)	γ_p (nm)	A_j	λ_j (nm)	γ_j (nm)	Φ_j (nm)
Value 1	1.129	213.67	4849.8	33.086	1082.3	1153.2	− 0.25722
Value 2				1.659	496.5	2559.7	0.83533

Table 3 Parameters of the Drude-CP dispersion formula for chromium [35]

2.2.3 Chromium

The dispersion of the adhesion chromium layer can be described by the complex dielectric function given by the Drude-critical point (CP) model [35]:

$$\varepsilon_{Cr}(\lambda) = \varepsilon_\infty - \frac{1}{\lambda_p^2(1/\lambda^2 + i/\gamma_p\lambda)} + \sum_{j=1}^{2} \frac{A_j}{\lambda_j}\left[\frac{e^{i\phi_j}}{(1/\lambda_j - 1/\lambda - i/\gamma_j)} + \frac{e^{-i\phi_j}}{(1/\lambda_j + 1/\lambda + i/\gamma_j)}\right], \tag{9}$$

with the parameters listed in Table 3.

3 Structure optimization

The sensing properties of an SPR structure are determining factors in the sensor performance and depend on its structural parameters and optical properties. The plasmonic material and layer thickness shape the resonance dip in the spectral reflectance $R_p(\lambda)$. Therefore, it is pivotal to optimize the structure so the best sensing properties are achieved. However, the optimization has to be performed for a specific use of the sensor. For that reason, aqueous solutions of NaCl with varying mass concentration of NaCl in water in a range of 0–10 wt% are considered as an analyte. Furthermore, a spectral range of 1000–1900 nm is considered so that the reflectance spectrum can be resolved by a spectrometer operating in the NIR spectral range [28]. From the best-performing plasmonic materials, gold and silver were selected, and a combination of these two materials was chosen to form the bimetallic gold-silver plasmonic configuration. Moreover, the thickness of the bimetallic film in a range of 20–60 nm is considered with the gold layer thickness in a range of 20–40 nm and the silver layer thickness in a range of 0–20 nm. Firstly, RI sensitivity is investigated as a function of the thicknesses of both gold and silver layers. The RI sensitivity can be defined as:

$$S_n = \frac{\delta\lambda_r}{\delta n}, \tag{10}$$

where $\delta\lambda_r$ is a change in the resonant wavelength, which corresponds to the change in the position of the dip related to a change in the refractive index of the analyte δn.

At first, theoretical RI sensitivities for the angles of incidence $\theta = 64°$ and $\theta = 63°$ are shown in Fig. 2a and b, respectively, when distilled water is considered as an analyte.

Based on the surface plots, it can be observed that for the angle of incidence $\theta = 64°$, the RI sensitivity is the highest for the structures that are represented by the lower-left corner of Fig. 2a. However, if the angle of incidence is changed to $\theta = 63°$, the RI sensitivity nearly doubles, and the maximum can be observed in the lower-right corner of Fig. 2b. It is necessary to mention that each of these surface plots consists of 2646 reflectance dips interrogated, which provides easily visible results of an optimal structure in terms of RI sensitivity for refractive index $n_w = 1.3330$. Since the reflectance spectra are analyzed for aqueous solutions of NaCl
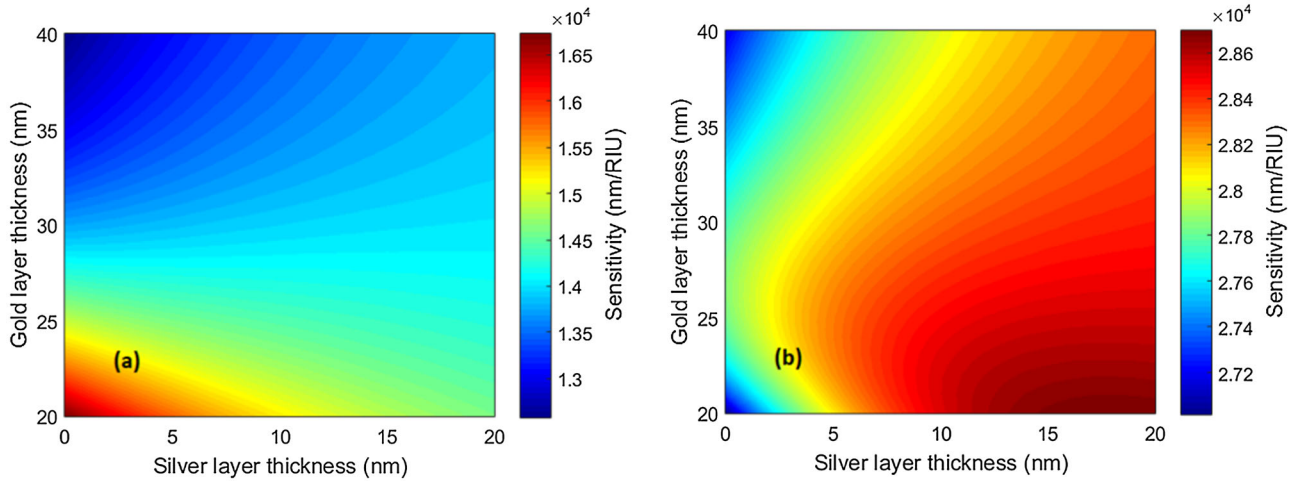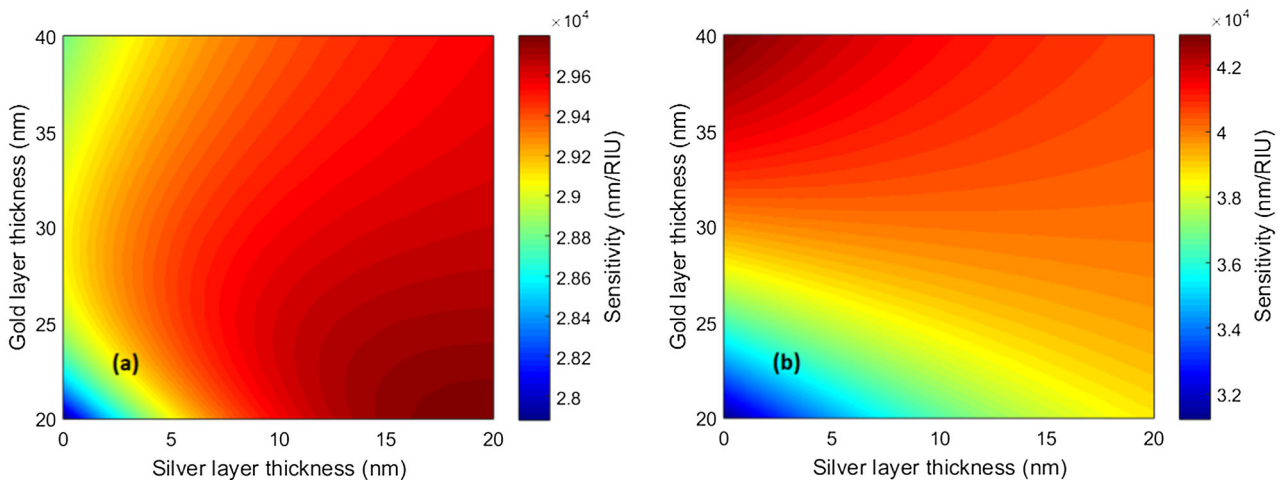
Fig. 2 Theoretical RI sensitivity as a function of the thicknesses of both gold and silver layers when distilled water is considered as an analyte for the angles of incidence $\theta = 64°$ (**a**) and $\theta = 63°$ (**b**)

with mass concentrations of 0–10 wt%, the RI of the analyte is in a range of 1.3330–1.3482. Therefore, the effect of changing the RI to the upper limit of the interval can be seen in Fig. 3a and b, respectively.

Similar behavior can be seen in terms of the magnitude of RI sensitivity. It is much higher for the angle of incidence $\theta = 63°$. However, it is evident that the optimal thickness parameters have changed significantly with changing the RI of the analyte.

Another property worth mentioning is the depth of the dip, which affects the figure of merit (FOM) defined as the sensitivity S_n divided by the full-width half-maximum (FWHM) of the dip. Accounting for the depth D of the dip related to the minimum spectral reflectance, the definition can be further expanded as [36]:

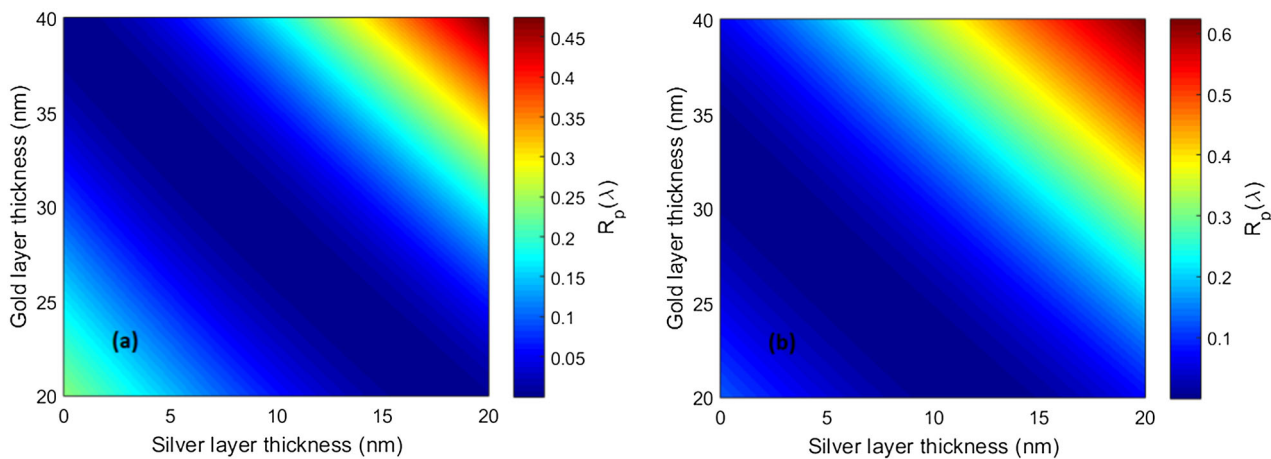$$\mathrm{FOM} = D\frac{S_n}{\mathrm{FWHM}}. \qquad (11)$$

Fig. 3 Theoretical RI sensitivity as a function of the thicknesses of both gold and silver layers when 10 wt% of NaCl in water is considered as an analyte for the angles of incidence $\theta = 64°$ (**a**) and $\theta = 63°$ (**b**)
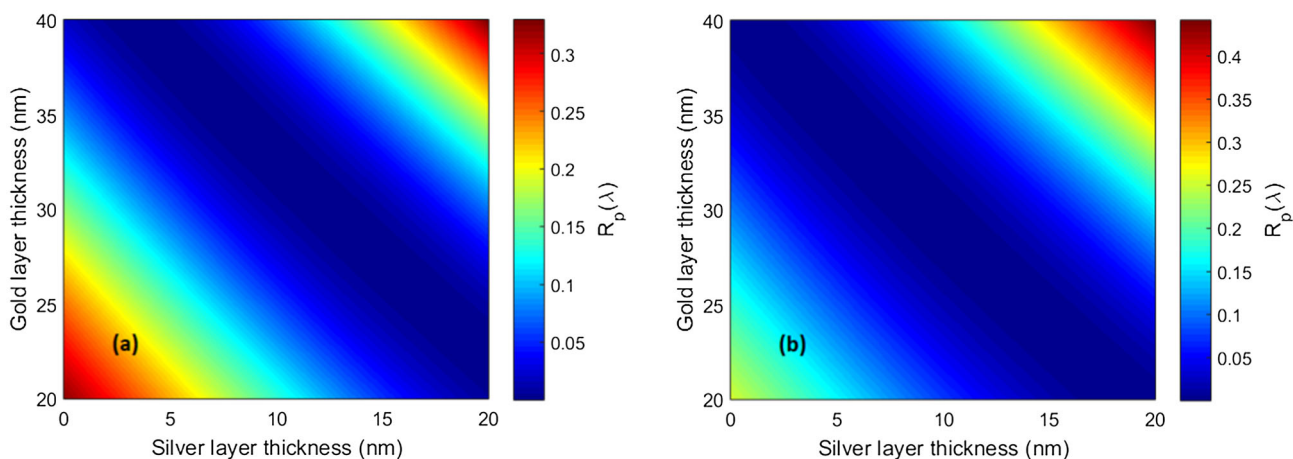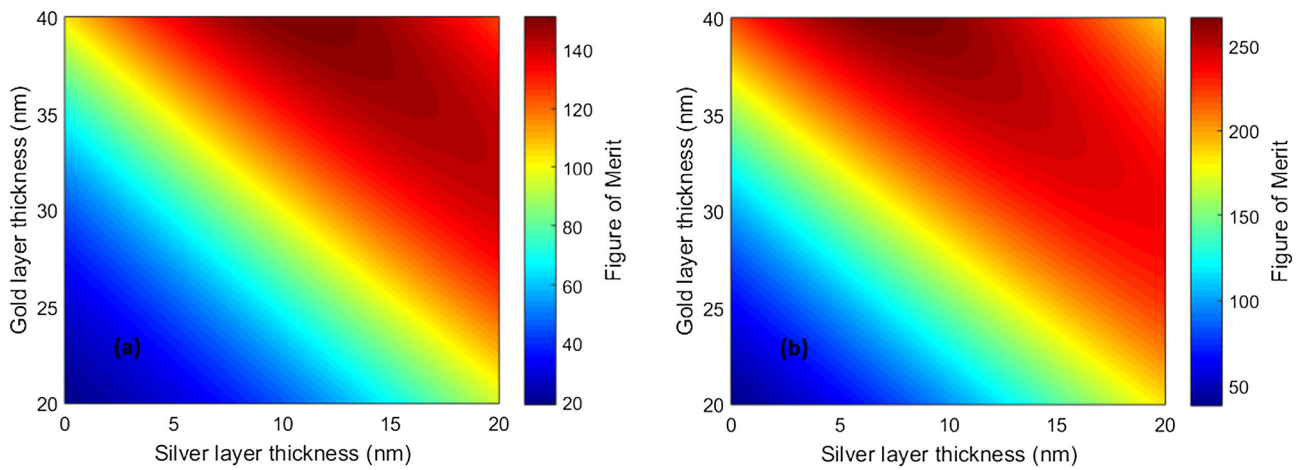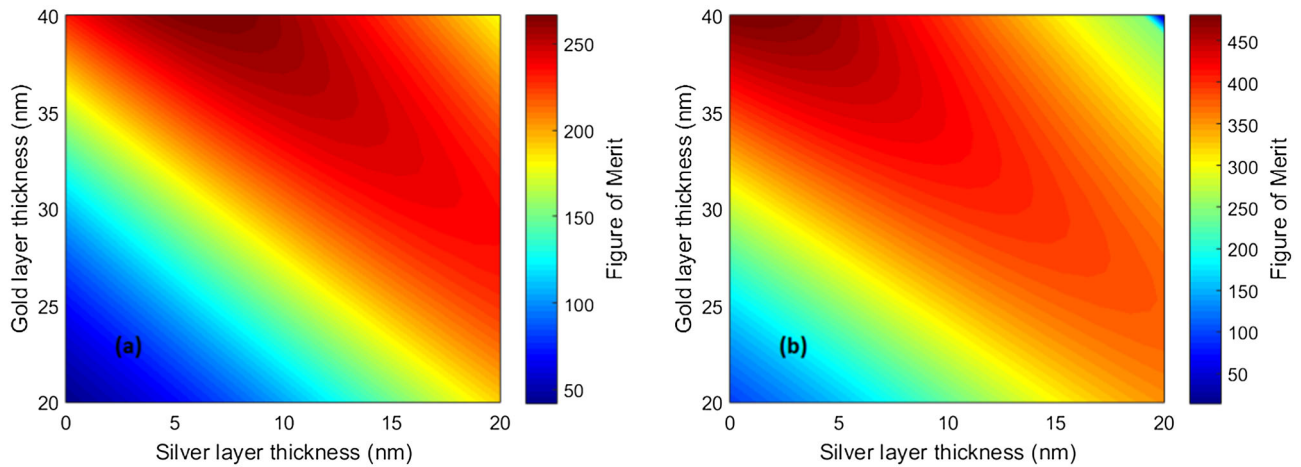
Fig. 4 Minimum reflectance as a function of the thicknesses of both gold and silver layers when distilled water is considered as an analyte for the angles of incidence $\theta = 64°$ (**a**) and $\theta = 63°$ (**b**)

The minimum reflectance for the angles of incidence $\theta = 64°$ and $\theta = 63°$ can be seen in Fig. 4a and b when distilled water is considered as an analyte.

The ideal thickness of the bimetallic film for the most pronounced dips is in the region of 40–45 nm for the angles incidence $\theta = 63°$ and $\theta = 64°$. Nevertheless, it changes with an increased RI of the analyte as the ideal thickness decreases. This behavior can be observed in Fig. 5a and b.

Fig. 5 Minimum reflectance as a function of the thicknesses of both gold and silver layers when 10 wt% of NaCl in water is considered as an analyte for the angles of incidence $\theta = 64°$ (**a**) and $\theta = 63°$ (**b**)

Fig. 6 Figure of merit as a function of the thicknesses of both gold and silver layers when distilled water is considered as an analyte for the angles of incidence $\theta = 64°$ (**a**) and $\theta = 63°$ (**b**)

To further investigate the performance of the SPR structure, the effect of FOM can be analyzed as well (Fig. 6). Despite the depth of the dip being a factor, the highest FOM can be achieved for the structures with the bimetallic film total thickness of 45–52 nm.

This shifts toward smaller thicknesses for the increased RI of the analyte, which can be seen in Fig. 7a and b, where the FOM is shown when 10 wt% of NaCl in water is considered as an analyte.

Fig. 7 Figure of merit as a function of the thicknesses of both gold and silver layers when 10 wt% of NaCl in water is considered as an analyte for the angles of incidence $\theta = 64°$ (**a**) and $\theta = 63°$ (**b**)
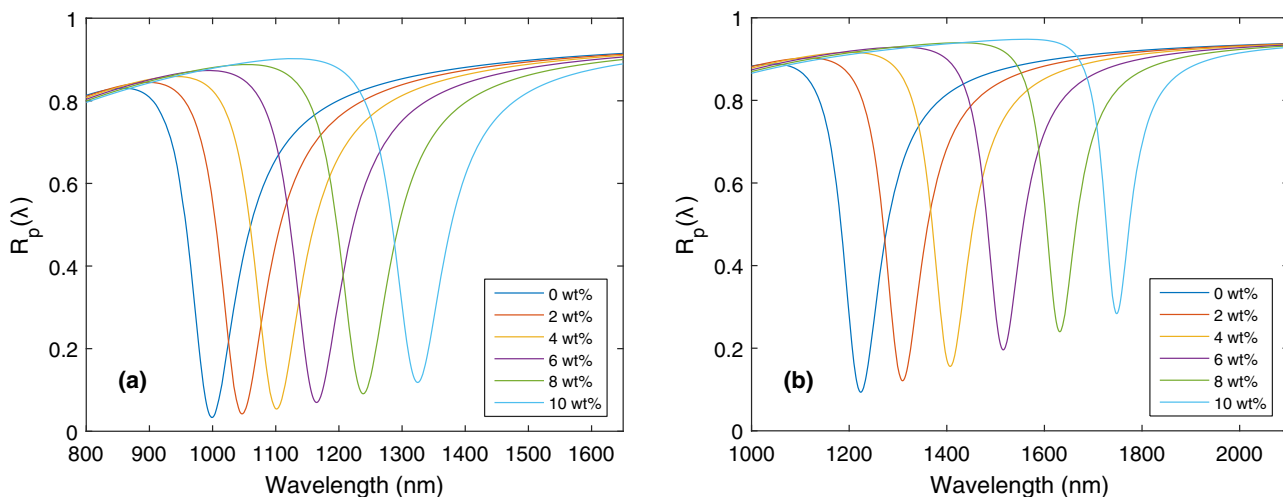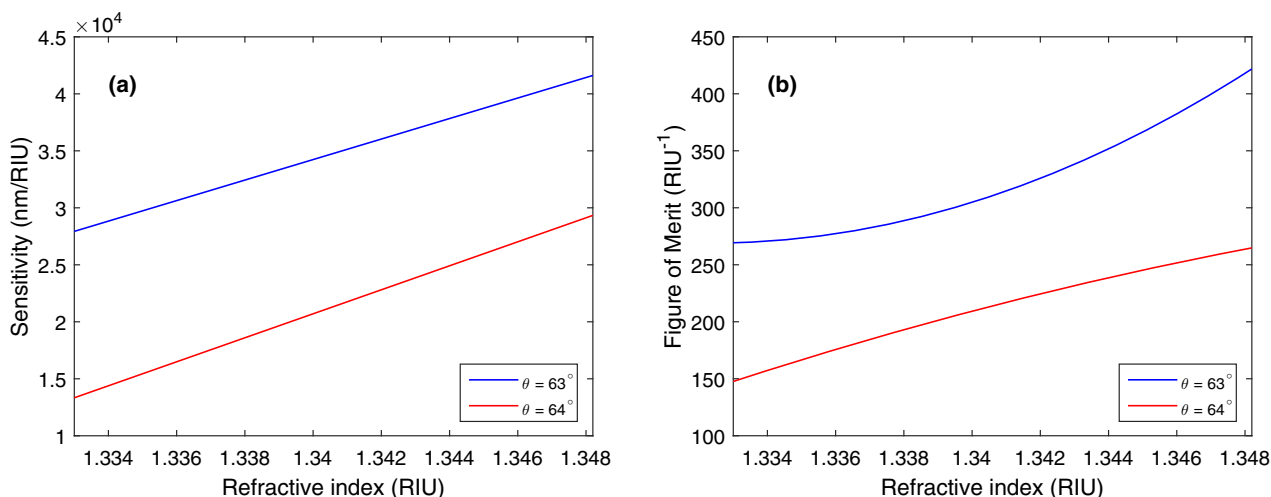
Fig. 8 Theoretical spectral reflectance $R_p(\lambda)$ for the gold layer thickness $t_{Au} = 40$ nm, the silver layer thickness $t_{Au} = 8$ nm, and the angles of incidence $\theta = 64°$ (**a**), $\theta = 63°$ (**b**). The aqueous solutions of 0–10 wt% NaCl in water are considered as an analyte

It is quite evident the FOM is the highest while gold is mostly dominant. However, sensitivity-wise, an ideal structure leans toward an increasing silver layer thickness. Therefore, a structure with the gold layer thickness $t_{Au} = 40$ nm and the silver layer thickness $t_{Au} = 8$ nm was selected to be further analyzed. Theoretical spectral reflectance $R_p(\lambda)$ for this structure and the angles of incidence $\theta = 64°$, $\theta = 63°$ is shown in Fig. 8a and b when the aqueous solutions of 0–10 wt% NaCl in water are considered as an analyte.

The dips are more shallow with an increasing RI of the analyte but they are also narrower. This is why the FOM values increase greatly despite the decreasing depth of the dip being taken into account. The shift of resonant wavelength is $\delta\lambda_r = 325$ nm for the angle of incidence $\theta = 64°$, and $\delta\lambda_r = 524$ nm for the angle of incidence $\theta = 63°$. A closer look at RI sensitivity and FOM as a function of the refractive index of the analyte is depicted in Fig. 9a and b, respectively.

It is apparent that the considered angle of incidence heavily impacts both RI sensitivity and FOM. However, further decreasing the angle of incidence would lead to a red shift in the resonant wavelength, and it would be pushed outside of the considered spectral range.

Achieved RI sensitivity for the selected structure and the angle of incidence $\theta = 64°$ varies in a range of 13,308–29,311 nm/RIU, and the highest figure of merit attains a value of 265.06 RIU^{-1}. For the angle of incidence $\theta = 63°$ RI sensitivity varies in a range of 27,912–41,592 nm/RIU, and the highest figure of merit attains a value of 424.46 RIU^{-1}.

Fig. 9 Theoretical RI sensitivity (**a**) and figure of merit (**b**) as a function of the refractive index of the analyte for the gold layer thickness $t_{Au} = 40$ nm, the silver layer thickness $t_{Au} = 8$ nm, and the angles of incidence $\theta = 64°$ (**a**), $\theta = 63°$ (**b**). The aqueous solutions of 0–10 wt% NaCl in water are considered as an analyte
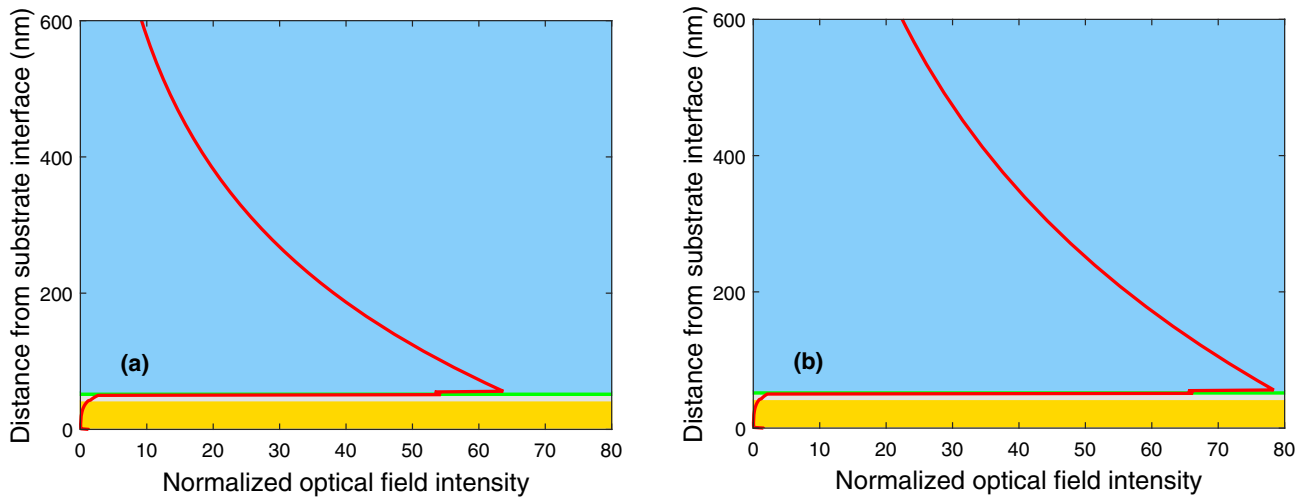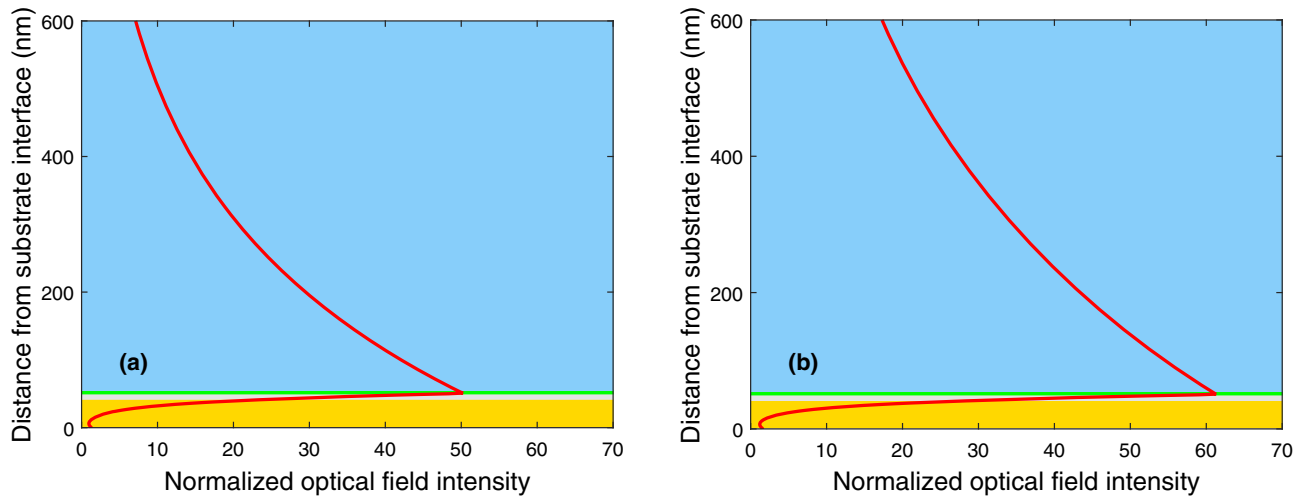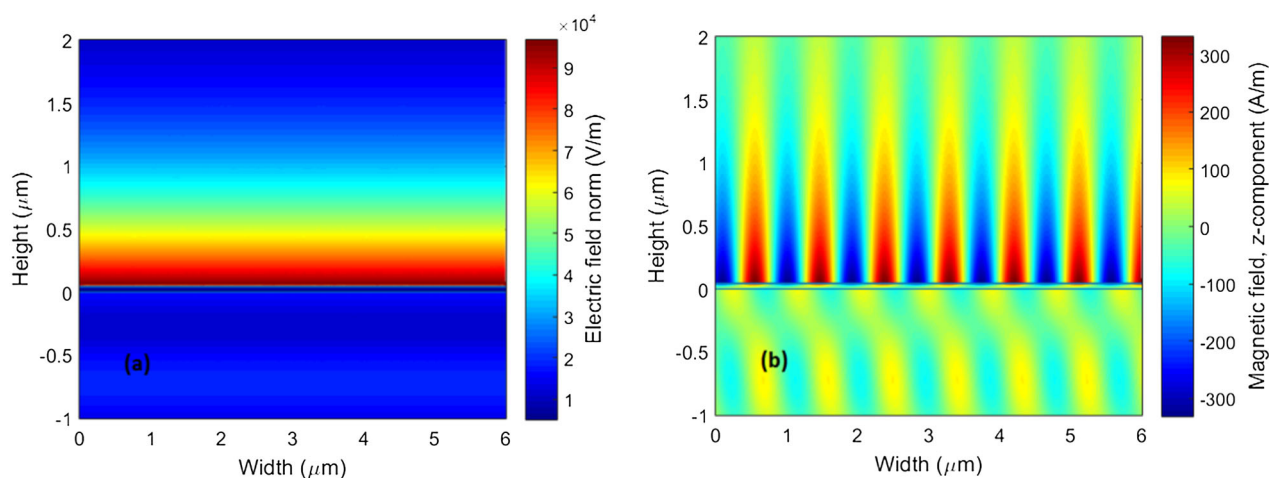
Fig. 10 Normalized optical field intensity for the electric field when distilled water is considered as an analyte for the gold layer thickness $t_{Au} = 40$ nm, the silver layer thickness $t_{Au} = 8$ nm, and the angles of incidence $\theta = 64°$ (**a**) and $\theta = 63°$ (**b**)

A more detailed description of the SPR effect at the analyte–bimetal interface can be provided by depicting the normalized optical field intensities. The normalized optical field intensity $|E_y|^2/|E_{y0}|^2$ in the structure at a wavelength of 999.04 nm is shown in Fig. 10a for the angle of incidence $\theta = 64°$ when the analyte is the distilled water, where E_{y0} is y component of the incident electric field that is parallel to the plane of incidence as evident from Fig. 1. Similarly, in Fig. 10b it is shown for $\theta = 63°$ at the resonance wavelength $\lambda_r = 1223.79$ nm.

It can be observed that the field enhancement is higher, and the evanescent tail appears larger in the analyte for the angle of incidence $\theta = 63°$, thus justifying higher sensitivity. Furthermore, the rate of the exponential decay of the field in the analyte appears to be slower for the angle of incidence $\theta = 63°$ marking larger penetration depth. Similar behavior can be seen in Fig. 11a and b for the magnetic field, showing the normalized optical field intensity $|H_z|^2/|H_{z0}|^2$.

Fig. 11 Normalized optical field intensity for the magnetic field when distilled water is considered as an analyte for the gold layer thickness $t_{Au} = 40$ nm, the silver layer thickness $t_{Au} = 8$ nm, and the angles of incidence $\theta = 64°$ (**a**) and $\theta = 63°$ (**b**)

Fig. 12 Electric field magnitude (**a**) and tangential component of the magnetic field (**b**) in the structure when distilled water is considered as an analyte for the gold layer thickness $t_{Au} = 40$ nm, the silver layer thickness $t_{Au} = 8$ nm, and the angle of incidence $\theta = 63°$

To confirm the theoretical results, the electric and magnetic field distributions in the structure were simulated in COMSOL Multiphysics. They are shown in Fig. 12 at the resonance wavelength $\lambda_r = 999.04$ nm for the angle of incidence $\theta = 63°$ when distilled water is considered as an analyte.

4 Conclusion

In this paper, a simple but highly sensitive bimetallic gold-silver SPR structure was proposed and its layer thicknesses were optimized based on reflectance spectra analysis. The gold-silver layer thickness ratio was varied, and a thorough analysis for aqueous solutions of NaCl was performed based on refractive index sensitivity, depth of the dip, and figure of merit. Due to the surface plots consisting of 2646 reflectance dips interrogated, easily visible results of an optimal structure were provided.

Based on this analysis, an optimized structure with the gold layer thickness $t_{Au} = 40$ nm and the silver layer thickness $t_{Au} = 8$ nm was selected, and the highest achieved RI sensitivity varied in a range of 27,912–41,592 nm/RIU with the highest figure of merit attaining a value of 424.46 RIU^{-1} for the angle of incidence $\theta = 63°$.

The structure proves to be of a simple design with a very high sensitivity to the refractive index of the analyte and a high figure of merit. It is possible to adjust the sensitivity by choosing a suitable angle of incidence. However, it is necessary to respect the spectrometer's spectral range. Despite choosing a liquid analyte as an example, the use of the structure can be extended to gaseous analytes as well. Furthermore, additions to the structure, for example, 2D materials such as graphene and black phosphorous are highly viable options due to a protective layer of silicon dioxide.

Data Availability Statement This manuscript has associated data in a data repository. [Authors' comment: The authors declare that the data and equations supporting the results of this study are available within the paper. The raw data sets generated during the current study are available from the corresponding author upon reasonable request.].

References

1. E. Kretschmann, H. Raether, Radiative decay of nonradiative surface plasmons excited by light. Z. Naturforschung **A23**, 2135–2136 (1968)
2. H. Raether, *Surface Plasmons on Smooth and Rough Surfaces and on Gratings* (Springer, New York, 1988)

3. J. Homola, S.S. Yee, G. Gauglitz, Surface plasmon resonance sensors: review. Sens. Actuators B Chem. **54**, 3–15 (1999)
4. J. Homola, *Surface Plasmon Resonance Based Sensors* (Springer, Berlin, 2006)
5. M. Manuel, B. Vidal, R. Lopéz, S. Alegret, J. Alonso-Chamarro, I. Garces, J. Mateo, Determination of probable alcohol yield in musts by means of an SPR optical sensor. Sens. Actuators B Chem. **11**, 455–459 (1993)
6. B. Liedberg, C. Nylander, I. Lundström, Principles of biosensing with an extended coupling matrix and surface plasmon resonance. Sens. Actuators B Chem. **11**, 63–72 (1993)
7. J. Dostálek, H. Vaisocherova, J. Homola, Multichannel surface plasmon resonance biosensor with wavelength division multiplexing. Sens. Actuators B Chem. **108**, 758–764 (2005)
8. H.R. Gwon, S.H. Lee, Spectral and angular responses of surface plasmon resonance based on the Kretschmann prism configuration. Mater. Trans. **51**, 1150–1155 (2010)
9. A. Shalabney, I. Abdulhalim, Figure-of-merit enhancement of surface plasmon resonance sensors in the spectral interrogation. Opt. Lett. **37**, 1175–1177 (2012)
10. P. Urbancova, J. Chylek, P. Hlubina, D. Pudis, Guided-mode resonance-based relative humidity sensing employing a planar waveguide structure. Sensors **20**, 6788 (2020)
11. P.I. Nikitin, A.A. Beloglazov, V.E. Kochergin, M.V. Valeiko, T.I. Ksenevich, Surface plasmon resonance interferometry for biological and chemical sensing. Sens. Actuators B Chem. **54**, 43–50 (1999)
12. S. Ruth, K.M. Woo, K.S. Hyun, K. Jang-Kyo, P.C. Yeong, P.T. Jung, Recent advances of bimetallic nanomaterials and its nanocomposites for biosensing applications. TrAC Trends Anal. Chem. **135**, 116159 (2021)
13. P.K. Maharana, S. Bharadwaj, R. Jha, Electric field enhancement in surface plasmon resonance bimetallic configuration based on chalcogenide prism. J. Appl. Phys. **114**, 014304 (2013)
14. G. AlaguVibisha, J.K. Nayak, P. Maheswari, N. Priyadharsini, A. Nisha, Z. Jaroszewicz, K.B. Rajesh, R. Jha, Sensitivity enhancement of surface plasmon resonance sensor using hybrid configuration of 2D materials over bimetallic layer of Cu-Ni. Opt. Commun. **463**, 125337 (2020)
15. H. Miaosen, L. Min, L. Ming-Yu, W. Xiaoyan, D. Shuo, L. Sisi, L. Haifei, Sensitivity enhancement of 2D material-based surface plasmon resonance sensor with an Al-Ni bimetallic structure. Sensors **23**, 1714 (2023)
16. W. Minghong, H. Yanyan, J. Shouzhen, Z. Chao, Y. Cheng, N. Tingyin, L. Xiaoyun, L. Chonghui, Z. Wenyuan, M. Baoyuan, Theoretical design of a surface plasmon resonance sensor with high sensitivity and high resolution based on graphene-WS2 hybrid nanostructures and Au-Ag bimetallic film. RSC Adv. **7**, 47177–47182 (2017)
17. R. Kumar, A.S. Kushwaha, M. Srivastava, H. Mishra, S.K. Srivastava, Enhancement in sensitivity of graphene-based zinc oxide assisted bimetallic surface plasmon resonance (SPR) biosensor. Appl. Phys. A **124**, 235 (2018)
18. L. Liu, M. Wang, L. Jiao, T. Wu, F. Xia, M. Liu, W. Kong, L. Dong, M. Yun, Sensitivity enhancement of a graphene-barium titanate-based surface plasmon resonance biosensor with an Ag-Au bimetallic structure in the visible region. J. Opt. Soc. Am. B **36**, 1108–1116 (2019)
19. Z. Pengyu, J. Wan, C. Guoquan, S. Jian, L. Chaoyang, T. Tang, A high-sensitivity SPR sensor with bimetal/silicon/two-dimensional material structure: a theoretical analysis. Photonics **8**, 270 (2021)
20. A. Yadav, A. Kumar, P. Sharan, Sensitivity enhancement of a plasmonic biosensor for urine glucose detection by employing black phosphorous. J. Opt. Soc. Am. B **39**, 200–206 (2022)
21. B. Karki, A. Pal, Y. Singh, S. Sharma, Sensitivity enhancement of surface plasmon resonance sensor using 2D material barium titanate and black phosphorus over the bimetallic layer of Au, Ag, and Cu. Opt. Commun. **508**, 127616 (2022)
22. A.K. Sharma, B.D. Gupta, On the performance of different bimetallic combinations in surface plasmon resonance based fiber optic sensors. J. Appl. Phys. **101**, 093111 (2007)
23. R. Tabassum, B.D. Gupta, SPR based fiber-optic sensor with enhanced electric field intensity and figure of merit using different single and bimetallic configurations. Opt. Commun. **367**, 23–34 (2016)
24. A.K. Sharma, G.J. Mohr, On the performance of surface plasmon resonance based fibre optic sensor with different bimetallic nanoparticle alloy combinations. J. Phys. D Appl. Phys. **41**, 055106 (2008)
25. B.H. Ong, X. Yuan, S.C. Tjin, J. Zhang, H.M. Ng, Optimised film thickness for maximum evanescent field enhancement of a bimetallic film surface plasmon resonance biosensor. Sens. Actuators B Chem. **114**, 1028–1034 (2006)
26. K.-S. Lee, T.S. Lee, I. Kim, W.M. Kim, Parametric study on the bimetallic waveguide coupled surface plasmon resonance sensors in comparison with other configurations. J. Phys. D Appl. Phys. **46**, 125302 (2013)
27. S. Chen, C. Lin, High-performance bimetallic film surface plasmon resonance sensor based on film thickness optimization. Optik **127**, 7514–7519 (2016)
28. J. Chylek, P. Maniakova, P. Hlubina, J. Sobota, D. Pudis, Highly sensitive plasmonic structures utilizing a silicon dioxide overlayer. Nanomaterials **12**, 3090 (2022)
29. P. Yeh, *Optical Waves in Layered Media* (John Wiley and Sons, Hoboken NJ, 2005)
30. I.H. Malitson, Interspecimen comparison of the refractive index of fused silica. J. Opt. Soc. Am. **55**, 1205–1209 (1965)
31. M.N. Polyanskiy, Refractive index database. http://refractiveindex.info
32. A. Vial, A.-S. Grimault, D. Macías, D. Barchiesi, M.L.D.L. Chapelle, Improved analytical fit of gold dispersion: application to the modeling of extinction spectra with a finite-difference time-domain method. Phys. Rev. B **71**, 085416 (2005)
33. R. Chlebus, J. Chylek, D. Ciprian, P. Hlubina, Surface plasmon resonance based measurement of the dielectric function of a thin metal film. Sensors **18**, 3693 (2018)
34. A.D. Rakić, A.B. Djurišić, J.M. Elazar, M.L. Majewski, Optical properties of metallic films for vertical-cavity optoelectronic devices. Optik **37**, 5271–5283 (1998)
35. A. Vial, T. Laroche, Description of dispersion properties of metals by means of the critical points model and application to the study of resonant structures using the FDTD method. J. Phys. D Appl. Phys. **40**, 7152–7158 (2007)
36. A. Sinibaldi, N. Danz, E. Descrovi, P. Munzert, U. Schulz, F. Sonntag, L. Dominici, F. Michelotti, Direct comparison of the performance of Bloch surface wave and surface plasmon polariton sensors. Sens. Actuators B Chem. **174**, 292–298 (2012)